

Article

Discovery of Novel Phosphodiesterase-2A Inhibitors by Structure-based Virtual Screening, Structural Optimization, and Bioassay

Chen Zhang, Ling-Jun Feng, Yiyu Huang, Deyan Wu, Zhe Li, Qian Zhou, Yinuo Wu, and Hai-Bin Luo

J. Chem. Inf. Model., **Just Accepted Manuscript** • DOI: 10.1021/acs.jcim.6b00551 • Publication Date (Web): 05 Jan 2017

Downloaded from <http://pubs.acs.org> on January 5, 2017

Just Accepted

“Just Accepted” manuscripts have been peer-reviewed and accepted for publication. They are posted online prior to technical editing, formatting for publication and author proofing. The American Chemical Society provides “Just Accepted” as a free service to the research community to expedite the dissemination of scientific material as soon as possible after acceptance. “Just Accepted” manuscripts appear in full in PDF format accompanied by an HTML abstract. “Just Accepted” manuscripts have been fully peer reviewed, but should not be considered the official version of record. They are accessible to all readers and citable by the Digital Object Identifier (DOI®). “Just Accepted” is an optional service offered to authors. Therefore, the “Just Accepted” Web site may not include all articles that will be published in the journal. After a manuscript is technically edited and formatted, it will be removed from the “Just Accepted” Web site and published as an ASAP article. Note that technical editing may introduce minor changes to the manuscript text and/or graphics which could affect content, and all legal disclaimers and ethical guidelines that apply to the journal pertain. ACS cannot be held responsible for errors or consequences arising from the use of information contained in these “Just Accepted” manuscripts.

Discovery of Novel Phosphodiesterase-2A Inhibitors by Structure-based Virtual Screening, Structural Optimization, and Bioassay

Chen Zhang^a, Ling-Jun Feng^a, Yiyong Huang^a, Deyan Wu^a, Zhe Li^a, Qian Zhou^a, Yinyu Wu^{a,*}, and

Hai-Bin Luo^{a,b,*}

^a School of Pharmaceutical Sciences, Sun Yat-Sen University, Guangzhou, 510006, China

^b Collaborative Innovation Center of High Performance Computing, National University of Defense

Technology, Changsha 410073, China

Abstract:

Phosphodiesterase-2A (PDE2A) is a potential therapeutic target for treatment of Alzheimer's disease and pulmonary hypertension. However, most of the current PDE2A inhibitors have the moderate selectivity over other PDEs. In the present study, we described the discovery of novel PDE2A inhibitors by structure-based virtual screening combining pharmacophore model screening, molecular docking, molecular dynamics simulations, and bioassay validation. Nine hits out of 30 molecules from the SPECS database (a hit rate of 30%) inhibited PDE2A with affinity less than 50 μ M. Optimization of compound **AQ-390/10779040** ($IC_{50} = 4.6 \mu$ M) from the virtual screening, which holds a novel scaffold of benzo[cd]indol-2(1H)-one among PDE inhibitors, leads to discovery of a new compound **LHB-8** with a significant improvement of inhibition ($IC_{50} = 570$ nM). The modeling studies demonstrated that **LHB-8** formed an extra hydrogen bond with Asp808 and a hydrophobic interaction with Thr768, in addition to the common interactions with Gln859 and Phe862 of PDE2A. The novel scaffolds discovered in the present study can be used for rational design of PDE2A inhibitors with high affinity.

1. Introduction

Phosphodiesterases (PDEs) are a super family of enzymes hydrolyzing the intracellular second messengers cyclic guanosine and adenosine monophosphate (cGMP and cAMP).^[1-2] It has been shown that decreased cGMP and cAMP concentrations are the main courses of certain diseases. PDEs, for their modulation of the level of cGMP and cAMP, are thus potential therapeutic targets for treatment of many diseases.^[3-5] Several PDEs inhibitors have been approved as clinical drugs. For example, sildenafil (a PDE5 inhibitor) is widely used for treatment of male erectile dysfunction and pulmonary hypertension.^[6-9]

Human PDEs are encoded by 21 genes and divided into 11 families which have different substrate specificity. Nevertheless, they share structural similarity in catalytic domains and possess a highly conserved hydrophobic clamp and bimetal ion binding center at the active sites.^[1,10-11] PDE2 is a dual-specific enzyme that hydrolyzes both cGMP and cAMP,^[12] and mostly distributes in the central nervous system (CNS), with relatively low expression in peripheral tissues. Several studies demonstrated that PDE2 modulates neuronal signalings involved in emotion, perception, concentration, learning and memory, thus made it a potential therapeutic target for treatment of CNS diseases such as Alzheimer's disease, mild cognitive impairment, and depression.^[13-14]

Although several efficient PDE2 inhibitors have been developed in recent years, there is still no PDE2 inhibitor on the market now (Fig. S1. ESI).^[15-21] The first generation of PDE2 inhibitors is **EHNA**, which lacks the selectivity over other PDEs.^[15-16] **BAY-60-7550**, a specific PDE2 inhibitor with IC₅₀ of 2 nM, showed good curative effect on the rodent behavioral models in learning and memory, and improved the acquisition and consolidation phases of novel object memory in age-impaired rats.^[22] However, the pharmacokinetic properties of **BAY-60-7550** are poor, which limited its clinical application.^[17] Thus, discovery of novel PDE2 inhibitors is highly in demand.

Structure-based drug design has been considered as a rational strategy and widely applied in the drug discovery in recent years. The X-ray crystal structure of PDE2 in complex with **BAY-60-7550** was reported in 2013. It supported the conserved glutamine switch mechanism for substrates-PDEs binding and revealed that a hydrophobic pocket may play an important role in the improvement of

1 binding affinity and selectivity for PDE2.^[20-22] This structural evidence may contribute to the
2
3 computer-aided inhibitor design for PDE2. Herein, our work on discovery of novel PDE2 inhibitors
4
5 started from a structure-based virtual screening to select potential leads from the commercial
6
7 database SPECS. Nine hits out of 30 molecules (a hit rate of 30%) were identified to be PDE2
8
9 inhibitors by subsequent bioassay, 5 of which possess novel scaffolds. Further structural optimization
10
11 of **AG-390/10779040** led to a new compound **LHB-8**, giving an IC₅₀ of 570 nM. The novel scaffolds
12
13 for PDE2 inhibitors reported in this paper might be valuable for development of PDE2 selective
14
15 inhibitors.
16
17
18
19

20 **2. Methods and materials**

21 **2.1. Molecular modeling**

22
23
24
25 In the first step, a pharmacophore model was generated for an expeditious screening of the
26
27 small-molecule database SPECS, in order to significantly reduce the size of the database. In the
28
29 second step, molecular docking was applied for a preliminary prediction of binding modes and
30
31 energies between the protein and molecules. The molecules in the dataset were further reduced in
32
33 this step. In the last step, molecular dynamics (MD) simulations, together with the molecular
34
35 mechanism/Poisson-Boltzman surface area (MM-PBSA) method^[23-25] were performed for a more
36
37 precise prediction of binding modes and corresponding binding energies. The 30 molecules with
38
39 proper binding patterns and top binding energies made up the final dataset, followed by subsequent
40
41 enzymatic bioassay.
42
43
44

45 **2.1.1. Database preparation**

46
47 The database SPECS (<http://www.specs.net>), consisting of almost 200,000 small molecules, was
48
49 selected for our virtual screening and filtered by Lipinski's Rule of Five^[26] using the modeling
50
51 software Molecular Operating Environment (MOE 2008.10), to form the initial dataset **Dataset0**.
52
53 Then multiple conformations for compounds were generated with the "conformation import" method
54
55 in MOE.
56
57

58 **2.1.2. Structure-based virtual screening**

1 Crystal structures of PDE2A with bound inhibitors were used to build a well-performed 3D
2 pharmacophore model for screening of **Dataset0**. Five crystal structures were downloaded from
3 Protein Data Bank (PDB ID: 4HTX, 4JIB, 4D08, 4D09, and 4C1I)^[20-22, 27] and applied to establish
4 the pharmacophore model. On basis of superposition of these five crystal structures, the spatial
5 positions and interactions between the ligands and the protein were carefully analyzed and common
6 structures in ligands such as aromatic rings, hydrophobic side chains, hydrogen bond donor and
7 acceptor groups were defined as pharmacophore features. The volume of the amino acid residues was
8 also applied as an exclusion feature to filter the compounds in the dataset. A test set, consisting of 30
9 active compounds ($IC_{50} < 10 \mu M$) and 174 inactive compounds ($IC_{50} \geq 10 \mu M$) which were
10 randomly picked from the ChEMBL database (<http://www.ebi.ac.uk/chembl>), was built for the
11 Goodness of hit (GH) test.^[28] The resulting pharmacophore model was utilized to filter compounds
12 in **Dataset0** and to save as **Dataset1**.

13
14
15
16
17
18
19
20
21
22
23
24
25
26
27
28
29
30
31
32
33
34
35
36
37
38
39
40
41
42
43
44
45
46
47
48
49
50
51
52
53
54
55
56
57
58
59
60
The false positive compounds in virtual screening may interfere with other detecting methods,
leading to fake hits or lead compounds.^[29] Thus, PAINS (pan-assay interfering compound
substructures) screening was applied to removing possible false positive compounds to build up
Dataset2.

Molecular docking was performed for the compounds in **Dataset2**. Those with higher scores
than the reference thresholds and optimal binding patterns made up **Dataset3**. Worthy to be
mentioned is that the invariant residue Gln859 in the binding pocket may have two conformations for
its side chain, as depicted in Fig. S2. Thus, two crystal structures (4HTX and 4C1I) were utilized as
reference structures for molecular docking. The two metal ions in the binding pocket were kept as it
is in the crystal structures of PDE families.^[1-3] Water molecules coordinating the two metal ions were
also retained after which hydrogen atoms were complemented by using H++ webserver
(<http://biophysics.cs.vt.edu/>) and protonation states were corrected.

Next, MD simulations were carried out to more precisely predict their binding patterns. The
software AMBER 10.0^[30] was used to simulate binding of molecules in **Dataset3** with PDE2A. The

docking poses of molecules in **Dataset3** were first calculated for the partial atomic charges by using the Hartree-Fock method at the 6-31G* level with Gaussian 03^[31]. Then Antechamber^[32] was applied to fit the restricted electrostatic potential (RESP) and assign the general amber force field (GAFF) parameters. The amber03 force field was utilized for this protein. The force field parameters for Zn²⁺ and Mg²⁺ were assigned with the "non-bond model" method.^[33] This simple model reproduced the structural and energetic properties of the solvated ions in MD simulations. The results of simulations agreed with experimental results in general^[34] in this and our previous study.^[33, 35] His660 and His696, which coordinate with two metal ions, were protonated at the δ positions. The oxygen atom bridging the two metal ions was treated as a hydroxide ion. His656, which is closest to the hydroxide ion and able to capture a proton, is treated as HIP (protonated histidine). An 8 Å TIP3P water box in the form of a truncated octahedron with Na⁺ (for 4HTX) or Cl⁻ (for 4C11) ions was added for neutralizing.

Such modified ligands and protein were then submitted to MD simulations. Eight ns MD simulations were carried out in the *NPT* ensemble with a constant pressure of 1 atm and a constant temperature of 300 K. The periodic boundary conditions were adopted, along with a 8 Å cutoff for long-range electrostatic interactions with the partial mesh Ewald (PME) method.^[36-37] The SHAKE algorithm^[38-39] were utilized for restriction of all bonds involving hydrogen atoms, and thereby the time step was set to 2 fs. Since the graphics processing units (GPUs) are available in performing floating-point calculations, an Intel Xeon E5620 CPU and an NVIDIA Tesla C2050 GPU were applied to accelerate the process of MD simulations for each system. Subsequent routine included the extraction of 100 snapshots of the last 1 ns trajectories and MM-PBSA binding free energy calculations with default parameters assigned.

In light of the MM-PBSA method^[23-25, 40-42], the binding free energy (ΔG_{bind}) can be calculated by the following equation 1: in which G_{comp} , G_{rec} and G_{lig} represent the free energies of complex, receptor and ligand, respectively.

$$\Delta G_{\text{bind}} = G_{\text{comp}} - G_{\text{rec}} - G_{\text{lig}} \quad (1)$$

G_{comp} is calculated by the sum of the MM energy E_{MM} , the solvation free energy $G_{\text{solv, comp}}$, and

the entropy contribution S_{com} , by equation 2. The same calculation can be applied to G_{rec} and G_{lig} .

$$G_{\text{comp}} = E_{\text{MM}} + G_{\text{solv, comp}} - TS_{\text{com}} \quad (2)$$

Equation 3 can be obtained from above:

$$\Delta G_{\text{bind}} = \Delta E_{\text{MM}} + \Delta G_{\text{solv}} - T\Delta S \quad (3)$$

ΔE_{MM} represents the gas phase interaction energy and can be decomposed into $E_{\text{MM, comp}}$, $E_{\text{MM, rec}}$ and $E_{\text{MM, lig}}$. Solvation free energy can be represented by the sum of the electrostatic solvation free energy and nonpolar solvation free energy. The electrostatic solvation free energy, ΔG_{PB} , can be calculated by the Poisson Boltzmann (PB) equation, while the nonpolar solvation free energy is proportional to the solvation accessible surface area (SASA) and is calculated by the following equations:

$$\Delta G_{\text{solv}} = \Delta G_{\text{PB}} + \Delta G_{\text{np}} \quad (4)$$

$$\Delta G_{\text{np}} = \gamma \text{SASA} + b \quad (5)$$

The calculation of the entropy contribution for the PDE2-ligand complexes was omitted, since it is extremely time-consuming for large protein-ligand systems.

After MD simulations, the compounds in **Dataset3** with negative binding energies at top rank and optimal binding patterns as inspected visually formed **Dataset4**. Finally, all of the compounds in **Dataset4** were purchased from SPECS and subjected to bioassay for their inhibition on PDE2A.

2.2. Bioassay

2.2.1. Protein expression and purification

The recombinant pET15b-PDE2A plasmid for expression of the catalytic domain (residues 580-919) was subcloned and purified following protocols previously reported^[34, 43-46], and was transferred into *E. coli* strain BL21 (Codonplus, Stratagene). The *E. coli* cells carrying the recombinant plasmid were grown in an 2XYT medium (containing 100 $\mu\text{g}/\text{mL}$ ampicillin and 20 $\mu\text{g}/\text{mL}$ chloramphenicol) at 37 °C until $\text{OD}_{600} = 0.6-0.8$. Then, 0.1 mM isopropyl- β -D-thiogalactopyranoside was added to induce the PDE2A protein expression at 16 °C for 24 h. The nickel nitriloacetic acid (Ni-NTA) column (Qiagen) was used to purify PDE2A proteins. The concentration of the PDE2 fractions was estimated according to the absorbance at 280 nm (calculated by the ProtParam software). A typical batch of purification yielded 10–20 mg PDE2A

1 protein from a 1.0 L cell culture. The PDE2A proteins had purity greater than 90% as shown by
2
3 SDS-PAGE.

4 5 **2.2.2. Enzymatic assays**

6
7 The enzymatic activities of the catalytic domain of PDE2A were measured with ^3H -cGMP as
8
9 the substrate in buffer of 50 mM Tris pH = 8.0, 10 mM MgCl_2 and 0.5 mM dithiothreitol, 20,000 -
10
11 30,000 cpm ^3H -cGMP per assay. Inhibitors solution (DMSO) in different concentration was added to
12
13 PDE2A enzyme. The enzymatic reaction was performed at room temperature of 25 °C for 15 min
14
15 and then terminated by addition of 0.2 M ZnSO_4 . The reaction product was precipitated out by 0.2 N
16
17 $\text{Ba}(\text{OH})_2$ and the unreacted ^3H -cGMP remained in the supernatant. The radioactivity in the
18
19 supernatant was measured in 2.5 ml of Ultima Gold liquid scintillation cocktails (PerkinElmer) by a
20
21 PerkinElmer 2910 liquid scintillation counter. At least eight concentrations of inhibitors were used
22
23 for measurement of inhibitors IC_{50} value. Each measurement was repeated three times, and IC_{50}
24
25 values were calculated by nonlinear regression. The mean values of the measurements were
26
27 considered as the final IC_{50} values with the SD values of the measurements. In this assay, **EHNA**
28
29 purchased from SIGMA was used as the reference compound.
30
31
32

33 34 **2.3. General chemistry**

35
36 ^1H NMR and ^{13}C NMR spectra were recorded on a BrukerBioSpin GmbH spectrometer at 400.1
37
38 and 100.6 MHz, respectively. Coupling constants are given in Hz. High-resolution mass spectra
39
40 (HRMS) were obtained on an IT-TOF mass spectrometer. Flash column chromatography was
41
42 performed using silica gel (200–300 mesh) purchased from Qingdao Haiyang Chemical Co. Ltd.
43
44 Thin-layer chromatography was performed on precoated silica gel F-254 plates (0.25 mm, Qingdao
45
46 Haiyang Chemical Co. Ltd) and visualized with UV light. All the starting materials and reagents
47
48 were purchased from commercial suppliers and used directly without further purification.
49
50

51 52 **2.3.1. General procedures^[47] for synthesis of compounds LHB-1 to LHB-8**

53
54 To the solution of Benzo[cd]indol-2(1H)-one (10 mmol) in CHCl_3 (30 mL), chlorosulfonic Acid
55
56 (30.0 mmol) was added dropwise in 10 min. The mixture was then stirred at room temperature for 6
57
58 h and poured into ice water to quench. The residue was extracted with 10 mL dichloromethane twice,
59
60

1 washed with brine, dried over anhydrous Na₂SO₄. The solvent was removed in vacuum to give the
2 crude product M1 (46%). The corresponding amine (1.2 mmol) was added to the **M1** (1 mmol) in
3 pyridine (10 mL). After the mixture was stirred at room temperature for 24 h, the reaction was
4 diluted with ethyl acetate, washed with saturated sodium bicarbonate solution, and brine, dried over
5 MgSO₄. The solvent was removed in vacuum. The crude product was purified by silica gel
6 chromatography with ethyl acetate/methanol (100:1) to give the final compound. Bioassay was then
7 performed for compounds **LHB-1** to **LHB-8** with the protocol described above.
8
9

16 2.3.2. *N*-(2-isopropylphenyl)-2-oxo-1,2-dihydrobenzo[cd]indole-6-sulfonamide (**LHB-1**)

17 Yellow solid, 68%; ¹H NMR (400 MHz, DMSO) δ 11.12 (s, 1H), 9.80 (s, 1H), 8.55 (d, *J* = 8.3
18 Hz, 1H), 8.10 (d, *J* = 6.9 Hz, 1H), 7.93 – 7.80 (m, 1H), 7.15 (d, *J* = 4.4 Hz, 1H), 7.06 – 6.96 (m, 1H),
19 6.91 (d, *J* = 7.8 Hz, 1H), 2.96 (dt, *J* = 13.6, 6.8 Hz, 1H), 0.67 (d, *J* = 6.8 Hz, 6H); ¹³C NMR (101
20 MHz, DMSO) δ 168.76, 145.75, 142.68, 132.64, 132.59, 130.26, 129.49, 128.64, 127.88, 127.27,
21 126.68, 126.18, 126.06, 125.86, 124.78, 124.54, 104.62, 26.48, 23.21; LC-MS (ESI), *m/z* for
22 C₂₀H₁₈N₂O₃S ([M - H]⁻): Calcd 365.43, found 365.4.
23
24
25
26
27
28
29
30
31

32 2.3.3. 2-oxo-*N*-(3,4,5-trimethoxyphenyl)-1,2-dihydrobenzo[cd]indole-6-sulfonamide(**LHB-2**)

33 Yellow solid, 53%; ¹H NMR (400 MHz, DMSO) δ 11.15 (s, 1H), 10.34 (s, 1H), 8.67 (d, *J* = 8.3
34 Hz, 1H), 8.16 (d, *J* = 7.6 Hz, 1H), 8.10 (d, *J* = 6.9 Hz, 1H), 7.94 (t, *J* = 7.7 Hz, 1H), 7.06 (d, *J* = 7.6
35 Hz, 1H), 6.31 (s, 2H), 3.57 (s, 6H), 3.50 (s, 3H); ¹³C NMR (101 MHz, DMSO) δ 169.21, 153.36,
36 143.56, 134.31, 133.86, 131.14, 129.53, 127.69, 127.23, 126.35, 125.43, 124.85, 105.13, 97.97,
37 60.50, 56.16; LC-MS (ESI), *m/z* for C₂₀H₁₈N₂O₆S ([M - H]⁻): Calcd 413.43, found 413.4.
38
39
40
41
42
43
44

45 2.3.4. *N*-(3,5-dichloro-4-hydroxyphenyl)-2-oxo-1,2-dihydrobenzo[cd]indole-6-sulfonamide 46 (**LHB-3**) 47

48 Yellow solid, 61%; ¹H NMR (400 MHz, DMSO) δ 11.20 (s, 1H), 10.53 (s, 1H), 10.04 (s, 1H),
49 8.62 (d, *J* = 8.4 Hz, 1H), 8.12 (d, *J* = 7.0 Hz, 1H), 8.07 (d, *J* = 7.6 Hz, 1H), 8.01-7.89 (m, 1H), 7.06
50 (d, *J* = 7.6 Hz, 1H), 6.96 (s, 2H); ¹³C NMR (101 MHz, DMSO) δ 169.16, 146.48, 143.82, 134.24,
51 131.31, 130.60, 129.31, 127.37, 127.01, 126.42, 125.55, 124.63, 123.01, 120.98, 105.16; LC-MS
52 (ESI), *m/z* for C₁₇H₁₀Cl₂N₂O₄S ([M - H]⁻): Calcd 408.24, found 408.2.
53
54
55
56
57
58
59
60

2.3.5. *N*-(3-chloro-4-fluorophenyl)-2-oxo-1,2-dihydrobenzo[*cd*]indole-6-sulfonamide (LHB-4)

Yellow solid, 81%; ^1H NMR (400 MHz, DMSO) δ 11.18 (s, 1H), 10.74 (s, 1H), 8.64 (d, $J = 8.3$ Hz, 1H), 8.16 – 8.07 (m, 2H), 7.96 (dd, $J = 8.4, 7.1$ Hz, 1H), 7.24 (t, $J = 9.1$ Hz, 1H), 7.16 (dd, $J = 6.5, 2.7$ Hz, 1H), 7.05 (d, $J = 7.6$ Hz, 1H), 6.98 (ddd, $J = 9.0, 4.1, 2.7$ Hz, 1H); ^{13}C NMR (101 MHz, DMSO) δ 169.16, 143.84, 134.40, 131.35, 129.27, 127.36, 126.99, 126.47, 125.54, 124.58, 118.59, 118.41, 116.49, 109.21, 109.01, 105.13; LC-MS (ESI), m/z for $\text{C}_{17}\text{H}_{10}\text{ClFN}_2\text{O}_3\text{S}$ ($[\text{M} - \text{H}]^-$): Calcd 375.79, found 375.7.

2.3.6. *N*-(3,4-difluorophenyl)-2-oxo-1,2-dihydrobenzo[*cd*]indole-6-sulfonamide (LHB-5)

Yellow solid, 72%; ^1H NMR (400 MHz, DMSO) δ 11.19 (s, 1H), 10.77 (s, 1H), 8.65 (d, $J = 8.4$ Hz, 1H), 8.12 (t, $J = 6.9$ Hz, 2H), 8.02 – 7.90 (m, 1H), 7.24 (dd, $J = 19.5, 9.2$ Hz, 1H), 7.11 – 7.00 (m, 2H), 6.84 – 6.76 (m, 1H); ^{13}C NMR (101 MHz, DMSO) δ 169.16, 143.84, 134.40, 131.35, 129.27, 127.36, 126.99, 126.47, 125.54, 124.58, 118.59, 118.41, 116.49, 109.21, 109.01, 105.13; LC-MS (ESI), m/z for $\text{C}_{17}\text{H}_{10}\text{F}_2\text{N}_2\text{O}_3\text{S}$ ($[\text{M} - \text{H}]^-$): Calcd 359.33, found 359.3.

2.3.7. *N*-(3,5-bis(trifluoromethyl)phenyl)-2-oxo-1,2-dihydrobenzo[*cd*]indole-6-sulfonamide (LHB-6)

Yellow solid, 62%; ^1H NMR (400 MHz, DMSO) δ 11.40 (d, $J = 57.7$ Hz, 1H), 11.21 (s, 1H), 8.65 (t, $J = 10.0$ Hz, 1H), 8.25 (t, $J = 10.0$ Hz, 1H), 8.11 (d, $J = 6.9$ Hz, 1H), 7.98 (dd, $J = 8.4, 7.1$ Hz, 1H), 7.66 (s, 1H), 7.60 (s, 2H), 7.09 (d, $J = 7.7$ Hz, 1H); ^{13}C NMR (101 MHz, DMSO) δ 169.05, 144.38, 140.22, 134.71, 131.83, 131.59, 131.50, 128.90, 127.43, 126.54, 126.30, 125.66, 124.60, 124.46, 121.89, 118.33, 116.84, 104.99; LC-MS (ESI), m/z for $\text{C}_{19}\text{H}_{10}\text{F}_6\text{N}_2\text{O}_3\text{S}$ ($[\text{M} - \text{H}]^-$): Calcd 459.35, found 459.3.

2.3.8. 4-amino-2-chlorophenyl 2-oxo-1,2-dihydrobenzo[*cd*]indole-6-sulfonate (LHB-7)

Yellow solid, 77%; ^1H NMR (400 MHz, DMSO) δ 11.17 (s, 1H), 10.20 (s, 1H), 10.06 (s, 1H), 8.63 (d, $J = 8.1$ Hz, 1H), 8.11 (d, $J = 6.4$ Hz, 1H), 8.04 – 7.89 (m, 2H), 7.02 (d, $J = 7.0$ Hz, 1H), 6.93 (s, 1H), 6.74 (s, 2H); ^{13}C NMR (101 MHz, DMSO) δ 169.18, 150.80, 143.48, 133.98, 131.09, 129.59, 127.57, 127.31, 126.38, 125.41, 124.78, 123.53, 122.10, 119.86, 117.25, 105.12; LC-MS (ESI), m/z for $\text{C}_{17}\text{H}_{11}\text{ClN}_2\text{O}_4\text{S}$ ($[\text{M} - \text{H}]^-$): Calcd 373.80, found 373.8.

2.3.9. 4-amino-3-chlorophenyl 2-oxo-1,2-dihydrobenzo[cd]indole-6-sulfonate (LHB-8)

Yellow solid, 81%, ^1H NMR (400 MHz, DMSO) δ 11.16 (s, 1H), 9.76 (s, 2H), 8.72 (d, $J = 8.4$ Hz, 1H), 8.14 (d, $J = 6.9$ Hz, 1H), 8.03 – 7.86 (m, 2H), 7.21 (d, $J = 8.5$ Hz, 1H), 7.03 (d, $J = 7.6$ Hz, 1H), 6.81 (dd, $J = 8.5, 2.4$ Hz, 1H), 6.70 – 6.59 (m, 1H). ^{13}C NMR (101 MHz, DMSO) δ 169.26, 152.46, 143.18, 133.11, 130.57, 130.52, 130.37, 129.01, 127.58, 127.07, 126.44, 125.15, 123.56, 119.20, 115.51, 104.95, 31.14. HRMS (ESI-TOF) m/z : $[\text{M} + \text{Na}]^+$ Calcd for $\text{C}_{17}\text{H}_{11}\text{N}_2\text{O}_4\text{SCl}$ 397.0020; Found 397.0030.

3. Results and discussion

3.1. Identification of PDE2 inhibitors with novel scaffolds by structure-based virtual screening and bioassay

A method combining pharmacophore model screening, molecular docking, molecular dynamics simulations was utilized to screen hits. The schematic diagram of the virtual screening strategy in this study is presented in Fig. 1.

Insert Fig. 1

The database SPECS of about 200,000 small molecules was pre-filtered by Lipinski's Rule of Five with the "conformation import" method in MOE 2008.10, leading to formation of **Dataset0** that contains 112,755 molecules passed the filtrations. **Dataset0** was rapidly screened by the pharmacophore model and then filtered by PAINS. Our initial pharmacophore model with 4 features was generated by the consensus strategy from the superposition of five PDE2A crystal structures (Fig. S6. ESI). However, too many molecules in **Dataset0** passed the pharmacophore screening and apparently this pharmacophore model is over-simplified. We manually modified the model by adding more features and performed the GH test by using known compounds. The pharmacophore model was tuned by 16 hits out of the 30 active compounds and 6 hits out of the 174 inactive compounds in the GH test set. The final GH test score of the pharmacophore model was 0.66, which is significantly better than 0.5, a threshold value regarded as a good model,^[48-50] thus implying that our pharmacophore model is suitable for screening purpose. The final pharmacophore model

1 contained 7 features and the exclusion feature, as shown in Fig. 2. After the pharmacophore
2 screening, 2,757 molecules fitted all the features in the model and were reserved as **Dataset1**.
3

4
5 *Insert Table 1 and Insert Fig. 2*
6

7 To avoid interference of false positive compounds with our subsequent screening, a PAINS
8 screening on compounds in **Dataset1** was performed using the online program Free AMDE-Tox
9 Filtering Tool (FAF-Drugs3, <http://fafdrugs3.mti.univ-paris-diderot.fr>),^[29] leading to 2,603 of the
10 2,757 compounds, which were deposited to **Dataset2**.
11
12
13
14

15 In order to obtain the optimal parameters for reliable molecular docking, the inhibitors in the
16 crystal structures (PDB ID: 4HTX and 4C1I) were redocked back to the structures. It turned out that
17 the Surflex-dock^[51] method embedded in TriposSybyl 2.0 was suitable for PDE2A. The average
18 RMSD values between the original X-ray pose and the top 10 docking poses were less than 1.5 Å for
19 the ligands **BAY-60-7550** and **EHNA**, implying the reliability of the docking. Thus, the identical
20 parameters were used for the docking screening of molecules in **Dataset2**. Fifty conformations were
21 randomly generated for each molecule. The means of top ten docking scores for 4HTX (11.13) and
22 4C1I (6.33) were used as the thresholds in the docking screening. Since the threshold of 11.13 for
23 4HTX was too high for most compounds in **Dataset2** to pass the docking screening, it was reduced
24 to 5.40 that was obtained from the test docking of the similar crystal structure 4JIB.
25
26
27
28
29
30
31
32
33
34
35
36
37

38 In the hydrophobic clamp of the catalytic site of PDE2, the substrate cAMP or cGMP was
39 sandwiched between Phe862 and Phe830 and formed hydrogen bonds with Gln859. Similar
40 interactions were also observed for competitive inhibitors of PDE2. Thus, Gln859 and Phe862 are
41 recognized as two conservative amino acid residues during the receptor–ligand recognitions. In
42 addition, the side chain of Gln859 may exist in two conformations, which induces distinct binding
43 patterns in the PDE2A crystal structures. Accordingly, both the crystal structures of 4HTX and 4C1I
44 were utilized during our docking screening. Only molecules fitting the pharmacophore model were
45 retained as potential PDE2 inhibitors. We chose the top 211 compounds (134 molecules based on the
46 crystal structure of 4HTX and 77 molecules based on 4C1I) in view of higher docking scores than
47 the thresholds and appropriate patterns to compose **Dateset3** for further study. The binding poses of
48
49
50
51
52
53
54
55
56
57
58
59
60

1 some molecules are shown in Fig. S3.

2
3 To evaluate the stability of each system of PDE2 in complex with small molecules, molecular
4 dynamics simulations were conducted in Amber 10.0. The results of 8 ns MD simulations and the
5 MM-PBSA binding free energy calculations with the stable trajectories implied that 30 systems met
6 the requirements sufficiently to cover both stable binding patterns and higher energies. The RMSD
7 values of the backbone atoms for 4HTX and 4C1I over MD simulations as references are shown in
8 Fig. S4. As a result, these 30 compounds were retained to constitute **Dataset4**. The RMSD curves
9 during MD simulations and predicted binding energies of the selected 30 compounds with PDE2A
10 are shown in Fig. S5 and Table S1.

11
12 The 30 compounds were purchased from SPECS for subsequent bioassay. EHNA was used as
13 the reference compound and has an IC_{50} of 2.6 μM which was comparable to the literature value of
14 0.8 μM ^[15]. Nine of 30 tested compounds were confirmed to be PDE2A inhibitors, and inhibited $\geq 50\%$
15 PDE2 activity at their 50 μM . Three of them even showed $\geq 50\%$ inhibition at their 10 μM (Fig.3).

16
17
18
19
20
21
22
23
24
25
26
27
28
29
30
31
32
33
34
35
36
37
38
39
40
41
42
43
44
45
46
47
48
49
50
51
52
53
54
55
56
57
58
59
60
Insert Fig. 3 and Fig. 4

3.2. New scaffolds for PDE2 inhibitors and their binding patterns during MD simulations

Among the 9 PDE2 inhibitors we identified, compound AG-690/12244899 gave the best IC_{50} for PDE2. However, its scaffold is similar to cAMP and cGMP^[52] and may have low selectivity over other PDE families. Thus, **AQ-390/10779040** and **AG-690/10776061**, which share the same novel scaffold of benzo[cd]indol-2(1H)-one, were selected for further structural modification. The inhibitory profiles of these two compounds with an unambiguous dose-dependent effect are shown in Fig. 4 (**AQ-390/10779040**, $IC_{50} = 4.6 \mu M$; **AG-690/10776061**, $IC_{50} = 9.8 \mu M$).

The binding modes of the new PDE2 inhibitors after 8 ns MD were analyzed for further structural modification. The predicted binding patterns of 4 new inhibitors are illustrated in Fig. 5. **AQ-390/10779040** and **AG-690/10776061** interact with PDE2A via two hydrogen bonds and π - π stacking interactions (picture 1 and picture 2, Fig. 5) The molecules are located in the hydrophobic clamp: residue Phe862, Gln859, Phe830 are on one end, while Leu770 and Ile866 form another side

1 (only Leu770 is shown in the figure). For **AG-670/40741585** (picture 3, Fig. 5), two hydrogen bonds
2 are formed with Gln859 and Tyr827, respectively. The π - π stacking against Phe862 is also observed.
3
4 The interactions between **AG-690/12244899** and PDE2A include two hydrogen bonds with Gln859
5 and a stack against Phe862 (picture 4, Fig. 5). Besides, the molecule stretches into the hydrophobic
6
7 pocket which was mentioned above.
8
9

10
11
12 *Insert Fig. 5*

13
14 In summary, the binding patterns of these four molecules are very similar. One or two hydrogen
15 bonds with Gln859 and π - π stacking with Phe862 are formed by all of them, which are commonly
16 considered as conservative interactions for PDE2 inhibitors. All but **AG-670/40741585** reach the
17 hydrophobic pocket in one end and occupy it. This binding mode may indicate a new way for
18 discovery of novel PDE2 inhibitors.
19
20
21
22
23

24 **3.3. Design and synthesis of potent PDE2 inhibitors with the benzo[cd]indol-2(1H)-one scaffold**

25
26 Based on our experimental results and the binding patterns analysis, we selected the scaffold of
27 **AQ-390/10779040** and **AG-690/10776061** for further structural modification (Scheme 1). According
28 to the binding modes, we kept the benzo[cd]indol-2(1H)-one core to retain the hydrogen bond
29 interaction with Gln859 and π - π stacking with Phe862, and initially focused on modification of the
30 phenyl group. We aimed to improve inhibition by adding interactions between the substituent groups
31 and PDE2.
32
33
34
35
36
37
38
39

40
41 *Insert Scheme 1*

42 Different substituent groups were attached to the phenyl group to explore the effect on the
43 inhibition (Table 2). Compared with **AQ-390/10779040** and **AG-690/10776061**, **LHB-1** and **LHB-2**
44 exhibited decrease in potency whereas six other compounds of **LHB-4** to **LHB-8** demonstrated
45 potency enhancement to a certain degree. We observed that the halogen groups on the phenyl group
46 improved inhibition while the methoxy or methyl groups didn't impact significantly. The best
47 compound was **LHB-8** giving the IC_{50} value of 570 nM, which exhibited 8-fold increase in the
48 potency to the hit compound **AQ-390/10779040**. The inhibitory profiles of these compounds clearly
49 showed dose-dependent pattern (Fig. S7). PAINS screening was applied to these derivatives and only
50
51
52
53
54
55
56
57
58
59
60

1 **LHB-3** failed to pass the test.

2
3 *Insert Table 2*

4 Molecular docking method was used to explore interactions of **LHB-8** with PDE2 for the
5 structure-activity relationship (SAR) analysis. The best docked pose of **LHB-8** from the
6 Surflex-dock method was selected and superposed on that of **AQ-390/10779040** (Fig.6). In addition
7 to the common interactions with Gln859 and Phe862, **LHB-8** forms an extra hydrogen bond with
8 Asp808. To further explore contribution of each component of **LHB-8** to the inhibition, the binding
9 free energy was calculated with the MM-PBSA method. Stable MD simulations trajectories were
10 utilized for data extracting and binding free energy calculating. The predicted binding free energies
11 were -29.00 and -32.23 kcal/mol for the complexes of PDE2-**AQ-390/10779040** and PDE2-**LHB-8**,
12 respectively, in agreement with their IC₅₀ values (4.6 μM and 0.57 μM). The energies for
13 electrostatic interaction (ΔG_{ele}) and polar contribution to solvation ($\Delta G_{\text{ele, sol}}$) of the complex of
14 PDE2- **LHB-8** are 6.8 and 5.2 kcal/mol lower than those for **AQ-390/10779040**. We speculated that
15 the polar contribution may play an important role for the enhanced inhibition.
16
17
18
19
20
21
22
23
24
25
26
27
28
29
30
31

32 *Insert Fig. 6*

33 Energy decomposition for the binding free energies was also performed to evaluate the
34 contribution of each residue in the binding pocket of PDE2 with the MM-PBSA method (Fig. 7).
35 Usually, a residue is considered to be important for recognition of ligands if the interaction energy
36 with ligand is lower than -1 kcal/mol. Our results suggest that the following residues may be
37 important for inhibition of **AQ-390/10779040** and **LHB-8** on PDE2: Ala771 (-2.51 and -2.49
38 kcal/mol), Asp808 (-1.33 and -1.94 kcal/mol), Ile826 (-1.45 and -1.63 kcal/mol), Phe830 (-1.65 and
39 -1.18 kcal/mol), Gln859 (-4.22 and -4.19 kcal/mol), Phe862 (-3.42 and -3.40 kcal/mol) and Ile866
40 (-0.93 and -0.95 kcal/mol). Among these residues, Gln859 and Phe862 mostly contributed to the total
41 binding free energies, in consistence with the binding patterns in which all ligands formed hydrogen
42 bonds with Gln859 and π - π stacking with Phe862. Thr768 and Asp808 in the hydrophobic pocket
43 made the major difference in energy contribution. Thr768 and Asp808 contribute to the PDE2-
44 **LHB-8** complex with the binding free energies of 0.7 and 0.6 kcal/mol lower than those of
45
46
47
48
49
50
51
52
53
54
55
56
57
58
59
60

1 PDE2-AQ-390/10779040, which is consistent with the previous result that the polar contribution
2
3 accounts for the improved inhibition against PDE2. From the MD binding patterns, one end of
4
5 **LHB-8** is located in the hydrophobic clamp and another end reached the hydrophobic pocket to form
6
7 a hydrogen bond with Asp808 (Fig. 6). Compared with AQ-390/10779040, **LHB-8** adopted a
8
9 slightly different conformation for stronger interaction with Thr768. The energy decomposition of
10
11 residues helps to interpret the binding patterns from the MD simulations and is supplementary to the
12
13 binding affinity results.
14

15
16 *Insert Fig. 7*
17
18
19

20 **4. Conclusions**

21
22 A structure-based virtual screening method combining pharmacophore model screening,
23
24 molecular docking, MD simulations, and bioassay was performed for discovery of novel PDE2A
25
26 inhibitors with new scaffolds in this study. Thirty compounds from the SPECS database were picked
27
28 out by the screening and 9 of them exhibited the inhibition of < 50 μM on PDE2. Five kinds of new
29
30 scaffolds were discovered out of the 9 hits. Structural optimization of AQ-390/10779040 ($\text{IC}_{50} = 4.6$
31
32 μM) led to discovery of a new compound **LHB-8** with an improved affinity of 570 nM. The strategy
33
34 we used in this study makes a good concession between computational cost and improvement of the
35
36 hit ratio of drug discovery and may have a wide application in further rational drug design.
37
38
39
40
41

42 ■ ASSOCIATED CONTENT

43 44 **Supporting Information**

45
46 The Supporting Information is available free of charge on the ACS Publications website.
47
48

49 ■ AUTHOR INFORMATION

50 51 **Corresponding Authors**

52
53 * E-mail: wyinuo3@mail.sysu.edu.cn (Y.W)

54
55 * E-mail: luohb77@mail.sysu.edu.cn; Fax: +86-20-3994 3000 (H.B.L.).
56
57
58

59 **Notes**

1 The authors declare no competing financial interest.
2
3
4

5 ■ Acknowledgements

6

7 This work was supported by Natural Science Foundation of China (81522041, 21572279, 81373258,
8 and 21402243), Guangdong Science Foundation (2014A020210009), Science Foundation of
9 Guangzhou City (2014J4100165), Research Fund for the Doctoral Program of Higher Education of
10 China (20130171110096), Fundamental Research Funds for the Central Universities (Sun Yat-Sen
11 University) (No. 13ykpy10), and Guangdong Province Higher Vocational Colleges & Schools Pearl
12 River Scholar Funded Scheme (2016). We also thank Special Program for Applied Research on Super
13 Computation of the NSFC-Guangdong Joint Fund (the second phase) for providing the
14 supercomputing service.
15
16
17
18
19
20
21
22
23
24
25
26

27 References

28

- 29
30 [1] Manallack, D. T.; Hughes, R. A.; Thompson, P. E. The next generation of phosphodiesterase
31 inhibitors: Structural clues to ligand and substrate selectivity of phosphodiesterases. *J. Med. Chem.*
32 **2005**, *48*, 3449-3462.
33
34 [2] Jeon, Y. H.; Heo, Y. S.; Kim, C. M.; Hyun, Y. L.; Lee, T. G.; Ro, S.; Cho, J. M.
35 Phosphodiesterase: overview of protein structures, potential therapeutic applications and recent
36 progress in drug development. *Cell. Mol. Life Sci.* **2005**, *62*, 1198-1220.
37
38 [3] Bender, A. T.; Beavo, J. A. Cyclic nucleotide phosphodiesterases: Molecular regulation to
39 clinical use. *Pharmacol. Rev.* **2006**, *58*, 488-520.
40
41 [4] Beavo, J. A.; Brunton, L. L. Cyclic nucleotide research - still expanding after half a century. *Nat.*
42 *Rev. Mol. Cell Bio.* **2002**, *3*, 710-718.
43
44 [5] Lugnier, C. Cyclic nucleotide phosphodiesterase (PDE) superfamily: A new target for the
45 development of specific therapeutic agents. *Pharmacol. Therapeut.* **2006**, *109*, 366-398.
46
47 [6] Setter, S. M.; Iltz, J. L.; Fincham, J. E.; Campbell, R. K.; Baker, D. E. Phosphodiesterase 5
48 inhibitors for erectile dysfunction. *Ann. Pharmacother.* **2005**, *39*, 1286-1295.
49
50
51
52
53
54
55
56
57
58
59
60

- [7] Liu, Y. G.; Shakur, Y.; Yoshitake, M.; Kambayashi, J. Cilostazol (Pletal (R)): A dual inhibitor of cyclic nucleotide phosphodiesterase type 3 and adenosine uptake. *Cardiovascular Drug Rev.* **2001**, *19*, 369-386.
- [8] Giembycz, M. A. Phosphodiesterase 4 inhibitors and the treatment of asthma - Where are we now and where do we go from here? *Drugs* **2000**, *59*, 193-212.
- [9] Zhu, J.; Mix, E.; Winblad, B. The antidepressant and Antiinflammatory effects of rolipram in the central nervous system. *Cns Drug Rev.* **2001**, *7*, 387-398.
- [10] Card, G. L.; England, B. P.; Suzuki, Y.; Fong, D.; Powell, B.; Lee, B.; Luu, C.; Tabrizizad, M.; Gillette, S.; Ibrahim, P. N.; Artis, D. R.; Bollag, G.; Milburn, M. V.; Kim, S. H.; Schlessinger, J.; Zhang, K. Y. J. Structural basis for the activity of drugs that inhibit phosphodiesterases. *Structure* **2004**, *12*, 2233-2247.
- [11] Beavo, J. A. Cyclic nucleotide phosphodiesterases: Functional implications of multiple isoforms. *Physiol. Rev.* **1995**, *75*, 725-748.
- [12] Conti, M.; Beavo, J. Biochemistry and physiology of cyclic nucleotide Phosphocliesterases: Essential components in cyclic nucleotide signaling. *Annu. Rev. Biochem.* **2007**, *76*, 481-511.
- [13] Boess, F. G.; Hendrix, M.; van der Staay, F. J.; Erb, C.; Schreiber, R.; van Staveren, W.; de Vente, J.; Prickaerts, J.; Blokland, A.; Koenig, G. Inhibition of phosphodiesterase 2 increases neuronal cGMP, synaptic plasticity and memory performance. *Neuropharmacology* **2004**, *47*, 1081-1092.
- [14] Martinez, S. E.; Wu, A. Y.; Glavas, N. A.; Tang, X. B.; Turley, S.; Hol, W. G. J.; Beavo, J. A. The two GAF domains in phosphodiesterase 2A have distinct roles in dimerization and in cGMP binding. *P. Natl. Acad. Sci. USA* **2002**, *99*, 13260-13265.
- [15] Podzuweit, T.; Nennstiel, P.; Mueller, A. Isozyme selective inhibition of cGMP-stimulated cyclic nucleotide phosphodiesterases by erythro-9-(2-Hydroxy-3-nonyl) adenine. *Cell. Signal.* **1995**, *7*, 733-738.
- [16] Rivet-Bastide, M.; Vandecasteele, G.; Hatem, S.; Verde, I.; Benardeau, A.; Mercadier, J.-J.; Fischmeister, R. CGMP-stimulated cyclic nucleotide phosphodiesterase regulates the basal calcium

1 current in human atrial myocytes. *J.Clin. Invest.* **1997**, *99*, 2710-2718.

2
3 [17]Rutten, K.; Prickaerts, J.; Hendrix, M.; van der Staay, F. J.; Sik, A.; Blokland, A.
4
5 Time-dependent involvement of cAMP and cGMP in consolidation of object memory: Studies using
6
7 selective phosphodiesterase type 2, 4 and 5 inhibitors. *Eur. J. Pharmacol.* **2007**, *558*, 107-112.

8
9 [18]Chambers, R. J.; Abrams, K.; Garceau, N. Y.; Kamath, A. V.; Manley, C. M.; Lilley, S. C.; Otte,
10
11 D. A.; Scott, D. O.; Sheils, A. L.; Tess, D. A.; Vellekoop, A. S.; Zhang, Y.; Lam, K. T. A new
12
13 chemical tool for exploring the physiological function of the PDE2 isozyme. *Bioorg. Med. Chem.*
14
15 *Lett.* **2006**, *16*, 307-310.

16
17 [19]Seybold, J.; Thomas, D.; Witzenrath, M.; Boral, S.; Hocke, A. C.; Burger, A.; Hatzelmann, A.;
18
19 Tenor, H.; Schudt, C.; Krull, M.; Schutte, H.; Hippenstiel, S.; Suttorp, N. Tumor necrosis
20
21 factor-alpha-dependent expression of phosphodiesterase 2: role in endothelial hyperpermeability.
22
23 *Blood* **2005**, *105*, 3569-3576.

24
25 [20]Buijnsters, P.; De Angelis, M.; Langlois, X.; Rombouts, F. J. R.; Sanderson, W.; Tresadern, G.;
26
27 Ritchie, A.; Trabanco, A. A.; VanHoof, G.; Van Roosbroeck, Y.; Andres, J.-I. Structure-Based
28
29 Design of a Potent, Selective, and Brain Penetrating PDE2 Inhibitor with Demonstrated Target
30
31 Engagement. *ACS Med. Chem. Lett.* **2014**, *5*, 1049-1053.

32
33 [21]Rombouts, F. J. R.; Tresadern, G.; Buijnsters, P.; Langlois, X.; Tovar, F.; Steinbrecher, T. B.;
34
35 Vanhoof, G.; Somers, M.; Andres, J.-I.; Trabanco, A. A. Pyrido[4,3-e][1,2,4]triazolo[4,3-a]pyrazines
36
37 as Selective, Brain Penetrant Phosphodiesterase 2 (PDE2) Inhibitors. *ACS Med. Chem. Lett.* **2015**, *6*,
38
39 282-286.

40
41 [22]Zhu, J.; Yang, Q.; Dai, D.; Huang, Q. X-ray Crystal Structure of Phosphodiesterase 2 in
42
43 Complex with a Highly Selective, Nanomolar Inhibitor Reveals a Binding-Induced Pocket Important
44
45 for Selectivity. *J. Am. Chem. Soc.* **2013**, *135*, 11708-11711.

46
47 [23]Massova, I.; Kollman, P. A. Combined molecular mechanical and continuum solvent approach
48
49 (MM-PBSA/GBSA) to predict ligand binding. *Perspect. Drug Discov.* **2000**, *18*, 113-135.

50
51 [24]Hou, T.; Wang, J.; Li, Y.; Wang, W. Assessing the Performance of the MM/PBSA and
52
53 MM/GBSA Methods. 1. The Accuracy of Binding Free Energy Calculations Based on Molecular
54
55

1 Dynamics Simulations. *J. Chem. Inf. Model.* **2011**, *51*, 69-82.

2
3 [25]Liu, M.; Yuan, M.; Luo, M.; Bu, X.; Luo, H.-B.; Hu, X. Binding of curcumin with glyoxalase I:
4 Molecular docking, molecular dynamics simulations, and kinetics analysis. *Biophys. Chem.* **2010**,
5 *147*, 28-34.

6
7
8
9 [26]Lipinski, C. A.; Lombardo, F.; Dominy, B. W.; Feeney, P. J., Experimental and computational
10 approaches to estimate solubility and permeability in drug discovery and development settings. *Adv.*
11 *Drug Del. Rev.* **1997**, *23*, 3-25.

12
13
14
15 [27]Plummer, M. S.; Cornicelli, J.; Roark, H.; Skalitzky, D. J.; Stankovic, C. J.; Bove, S.; Pandit, J.;
16 Goodman, A.; Hicks, J.; Shahripour, A.; Beidler, D.; Lu, X. K.; Sanchez, B.; Whitehead, C.; Sarver,
17 R.; Braden, T.; Gowan, R.; Shen, X. Q.; Welch, K.; Ogden, A.; Sadagopan, N.; Baum, H.; Miller, H.;
18 Banotai, C.; Spessard, C.; Lightle, S. Discovery of potent, selective, bioavailable phosphodiesterase
19 2 (PDE2) inhibitors active in an osteoarthritis pain model, Part I: Transformation of selective
20 pyrazolodiazepinone phosphodiesterase 4 (PDE4) inhibitors into selective PDE2 inhibitors. *Bioorg.*
21 *Med. Chem. Lett.* **2013**, *23*, 3438-3442.

22
23
24
25
26
27 [28]Osman, F. G. D.; Henry, R. Metric for analyzing hit lists and pharmacophores. In
28 *Pharmacophore Perception, Development, and Use in Drug Design*; Guner., O. F., Ed.; International
29 University Line: La Jolla, CA, 2000; pp 193-210.

30
31
32
33 [29]Baell, J. B.; Holloway, G. A. New Substructure Filters for Removal of Pan Assay Interference
34 Compounds (PAINS) from Screening Libraries and for Their Exclusion in Bioassays. *J. Med.*
35 *Chem.* **2010**, *53*, 2719-2740.

36
37
38
39 [30]Case, D. A.; Darden, T. A.; Cheatham, T. E. III; Simmerling, C. L.; Wang, J.; Duke, R. E.; Luo,
40 R.; Walker, R. C.; Zhang, W.; Merz, K. M.; Roberts, B. P.; Hayik, S.; Roitberg, A.; Seabra, G.;
41 Swails, J.; Götz, A. W.; Kolossváry, I.; Wong, K. F.; Paesani, F.; Vanicek, J.; Wolf, R. M.; Liu, J.;
42 Wu, X.; Brozell, S. R.; Steinbrecher, T.; Gohlke, H.; Cai, Q.; Ye, X.; Wang, J.; Hsieh, M. J.; Cui, G.;
43 Roe, D. R.; Mathews, D. H.; Seetin, M. G.; Salomon-Ferrer, R.; Sagui, C.; Babin, V.; Luchko, T.;
44 Gusarov, S.; Kovalenko, A.; Kollman, P. A. AMBER 10.0, University of California, San Francisco.

1 2008.

2
3 [31]Frisch, M. J.; Trucks, G. W.; Schlegel, H. B.; Scuseria, G. E.; Robb, M. A.; Cheeseman, J. R.;
4 Montgomery, J. A.; Vreven, T.; Kudin, K. N.; Burant, J. C.; Millam, J. M.; Iyengar, S. S.; Tomasi, J.;
5 Barone, V.; Mennucci, B.; Cossi, M.; Scalmani, G.; Rega, N.; Petersson, G.A.; Nakatsuji, H.; Hada,
6 M.; Ehara, M.; Toyota, K.; Fukuda, R.; Hasegawa, J.; Ishida, M.; Nakajima, T.; Honda, Y.; Kitao, O.;
7 Nakai, O.; Klene, M.; Li, X.; Knox, J. E.; Hratchian, H. P.; Cross, J. B.; Bakken, V.; Adamo, C.;
8 Jaramillo, J.; Gomperts, R.; Stratmann, R. E.; Yazyev, O.; Austin, A. J.; Cammi, R.; Pomelli, C.;
9 Ochterski, J. W.; Ayala, P. Y.; Morokuma, K.; Voth, G. A.; Salvador, P.; Dannenberg, J. J.;
10 Zakrzewski, V. G.; Dapprich, S.; Daniels, A. D.; Strain, M. C.; Farkas, O.; Malick, D. K.; Rabuck, A.
11 D.; Raghavachari, K.; Foresman, J. B.; Ortiz, J. V.; Cui, Q.; Baboul, A. G.; Clifford, S.; Cioslowski,
12 J.; Stefanov, B. B.; Liu, G.; Liashenko, A.; Piskorz, P.; Komaromi, I.; Martin, R. L.; Fox, D. J.;
13 Keith, T.; Al-Laham, M. A.; Peng, C. Y.; Nanayakkara, A.; Challacombe, M.; Gill, P. M. W.;
14 Johnson, B.; Chen, W.; Wong, M. W.; Gonzalez, C.; Pople, J. A. *Gaussian 03*, Revision E.01;
15 Gaussian, Inc.: Pittsburgh PA, 2004.

16
17 [32]Wang, J.; Wang, W.; Kollman, P. A.; Case, D. A. Automatic atom type and bond type
18 perception in molecular mechanical calculations. *J. Mol. Graph. Model.* **2006**, *25*, 247-260.

19
20 [33]Li, Z.; Cai, Y. H.; Cheng, Y. K.; Lu, X.; Shao, Y. X.; Li, X. S.; Liu, M.; Liu, P. Q.; Luo, H.-B.
21 Identification of Novel Phosphodiesterase-4D Inhibitors Prescreened by Molecular
22 Dynamics-Augmented Modeling and Validated by Bioassay. *J. Chem. Inf. Model.* **2013**, *53*,
23 972-981.

24
25 [34]Stote, R. H.; Karplus, M. Zinc binding in proteins and solution: A simple but accurate
26 nonbonded representation. *Proteins* **1995**, *23*, 12-31.

27
28 [35]Li, Z.; Lu, X.; Feng, L. J.; Gu, Y.; Li, X. S.; Wu, Y. U.; Luo, H. B. Molecular dynamics-based
29 discovery of novel phosphodiesterase-9A inhibitors with non-pyrazolopyrimidinone scaffolds. *Mol.*
30 *Biosyst.* **2015**, *11*, 115-125.

31
32 [36]Essmann, U.; Perera, L.; Berkowitz, M. L.; Darden, T.; Hsing, L.; Pedersen, L. G.A smooth
33
34
35
36
37
38
39
40
41
42
43
44
45
46
47
48
49
50
51
52
53
54
55
56
57
58
59
60

1 particle mesh Ewald method. *J. Chem. Phys.* **1995**, *103*, 8577-8593.

2
3 [37]Darden, T.; York, D.; Pedersen, L. Particle mesh Ewald: an N.log(N) method for Ewald sums in
4 large systems. *J. Chem. Phys.* **1993**, *98*, 10089-10092.

5
6
7 [38]Miyamoto, S.; Kollman, P. A. SETTLE: an analytical version of the SHAKE and RATTLE
8 algorithm for rigid water models. *J. Comput. Chem.* **1992**, *13*, 952-962.

9
10
11 [39]Ryckaert, J. P.; Ciccotti, G.; Berendsen, H. J. C. Numerical integration of the Cartesian
12 equations of motion of a system with constraints: molecular dynamics of n-alkanes. *J. Comput. Phys.*
13
14
15
16
17 **1977**, *23*, 327-341.

18
19 [40]Wang, J. M.; Hou, T. J.; Xu, X. J. Recent Advances in Free Energy Calculations with a
20 Combination of Molecular Mechanics and Continuum Models. *Curr. Comput-Aid. Drug* **2006**, *2*,
21
22
23
24 287-306.

25 [41]Xu, L.; Sun, H. Y.; Li, Y. Y.; Wang, J. M.; Hou, T. J. Assessing the Performance of MM/PBSA
26 and MM/GBSA Methods. 3. The Impact of Force Fields and Ligand Charge Models. *J. Phys. Chem.*
27
28
29
30
31 *B* **2013**, *117*, 8408-8421.

32 [42]Hou, T. J.; Wang, J. M.; Li, Y. Y.; Wang, W. Assessing the Performance of the Molecular
33 Mechanics/Poisson Boltzmann Surface Area and Molecular Mechanics/Generalized Born Surface
34 Area Methods. II. The Accuracy of Ranking Poses Generated From Docking. *J. Comput. Chem.*
35
36
37
38
39
40 **2011**, *32*, 866-877.

41 [43]Shao, Y. X.; Huang, M.; Cui, W.; Feng, L. J.; Wu, Y.; Cai, Y.; Li, Z.; Zhu, X.; Liu, P.; Wan, Y.;
42 Ke, H.; Luo, H.-B. Discovery of a phosphodiesterase-9A inhibitor as a potential hypoglycemic agent.
43
44
45
46
47 *J. Med. Chem.* **2014**, *57*, 10304-130313.

48 [44]Su, T.; Zhang, T.; Xie, S.; Yan, J.; Wu, Y.; Li, X.; Huang, L.; Luo, H.-B. Discovery of novel
49 PDE9 inhibitors capable of inhibiting A β aggregation as potential candidates for the treatment of
50
51
52
53 Alzheimer's disease. *Sci. Rep.* **2016**, *6*, 21826.

54 [45]Shang, N.N.; Shao, Y.X.; Cai, Y.H.; Guan, M.; Huang, M.; Cui, W.; He, L.; Yu, Y.J.; Huang, L.;
55
56
57
58
59
60 Li, Z.; Bu, X. Z.; Ke, H.; Luo, H.-B. Discovery of 3-(4-hydroxybenzyl)-1-(thiophen-2-yl)
chromeno[2,3-c]pyrrol-9(2H)-one as a phosphodiesterase-5 inhibitor and its complex crystal

1 structure. *Biochem. Pharmacol.* **2014**, *89*, 86-98.

2
3 [46]Meng, F.; Hou, J.; Shao, Y. X.; Wu, P. Y.; Huang, M.; Zhu, X.; Cai, Y. H.; Li, Z.; Xu, J.; Liu, P.
4
5 Q.; Luo, H.-B.; Wan, Y.; Ke, H. Structure-based discovery of highly selective phosphodiesterase-9A
6
7 inhibitors and implications for inhibitor design. *J. Med. Chem.* **2012**, *55*, 8549-8558.

8
9 [47]Xue, X.; Zhang, Y.; Liu, Z.; Song, M.; Xing, Y.; Xiang, Q.; Wang, Z.; Tu, Z.; Zhou, Y.; Ding,
10
11 K.; Xu, Y. Discovery of Benzo[cd]indol-2(1H)-ones as Potent and Specific BET Bromodomain
12
13 Inhibitors: Structure-Based Virtual Screening, Optimization, and Biological Evaluation. *J. Med.*
14
15 *Chem.* **2016**, *59*, 1565-1579.

16
17 [48]Vadivelan, S.; Sinha, B. N.; Irudayam, S. J.; Jagarlapudi, S. A. R. P. Virtual screening studies to
18
19 design potent CDK2-cyclin A inhibitors. *J. Chem. Inf. Model.* **2007**, *47*, 1526-1535.

20
21 [49]Boppana, K.; Dubey, P. K.; Jagarlapudi, S. A. R. P.; Vadivelan, S.; Rambabu, G. Knowledge
22
23 based identification of MAO-B selective inhibitors using pharmacophore and structure based virtual
24
25 screening models. *Eur. J. Med. Chem.* **2009**, *44*, 3584-3590.

26
27 [50]Shih, K.-C.; Lin, C.-Y.; Zhou, J.; Chi, H.-C.; Chen, T.-S.; Wang, C.-C.; Tseng, H.-W.; Tang,
28
29 C.-Y. Development of Novel 3D-QSAR Combination Approach for Screening and Optimizing
30
31 B-Raf Inhibitors in silico. *J. Chem. Inf. Model.* **2011**, *51*, 398-407.

32
33 [51]Jain, A. N. Surflex: Fully automatic flexible molecular docking using a molecular
34
35 similarity-based search engine. *J. Med. Chem.* **2003**, *46*, 499-511.

36
37 [52]Lim, F. P. L.; Dolzhenko, A. V. 1,3,5-Triazine-based analogues of purine: From isosteres to
38
39 privileged scaffolds in medicinal chemistry. *Eur. J. Med. Chem.* **2014**, *85*, 371-390.
40
41
42
43
44
45
46
47
48
49
50
51
52
53
54
55
56
57
58
59
60

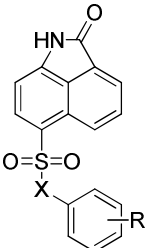
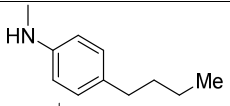
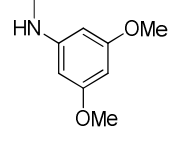
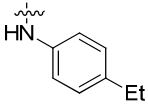
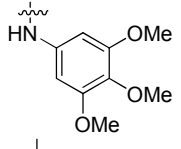
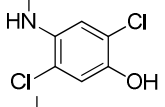
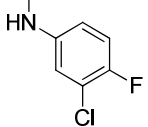
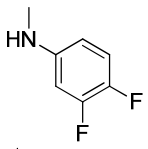
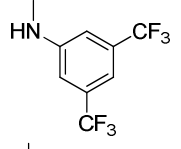
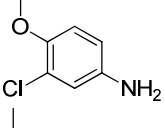
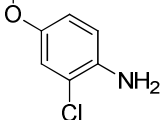
Table 1. Statistical parameters for the pharmacophore screening of the test set in the GH test.

Parameters	Value
Total molecules in dataset (D)	204
Total number of actives in dataset (A)	30
Total hits (H _t)	22
Active hits (H _a)	16
% Yield of actives [(H _a /H _t)*100]	72.7
% Ratio of actives [(H _a /A)*100]	53.3
Enrichment factor (EF) [(H _a *D)/(H _t *A)] ^a	4.95
False negatives [A-H _a]	14
False positives [H _t -H _a]	6
Goodness of hit test score(GH test score) ^b	0.66

^a $EF = (H_a * D) / (H_t * A)$.

^b $GH \text{ test score} = [H_a * (3A + H_t) / (4H_t * A)] * [1 - (H_t - H_a) / (D - A)]$.

Table 2. SAR of modified compounds based on the hit compounds **AQ-390/10779040** and **AG-690/10776061**.

Compound		PDE2A IC ₅₀ ^a (μ M)
AQ-390/10779040		4.62 ± 0.78
AG-690/10776061		9.78 ± 0.34
LHB-1		> 10
LHB-2		> 10
LHB-3		3.61 ± 0.39
LHB-4		1.83 ± 0.29
LHB-5		1.58 ± 0.29
LHB-6		0.98 ± 0.29
LHB-7		2.91 ± 0.34
LHB-8		0.57 ± 0.03

^a EHNA was used as the reference compound with an IC₅₀ of 2.60 μ M.

Table 3. Predicted free energies (kcal/mol) for binding of **AQ-390/10779040** or **LHB-8** to human PDE2 by the MM-PBSA method.

Energy Terms (kcal/mol)	AQ-390/10779040	LHB-8
$\Delta G_{\text{ele}}^{\text{a}}$	-22.61 ± 2.45	-29.38 ± 3.37
$\Delta G_{\text{vdw}}^{\text{b}}$	-37.74 ± 2.55	-39.45 ± 2.36
$\Delta G_{\text{nonpol, sol}}^{\text{c}}$	-4.06 ± 0.12	-4.00 ± 0.11
$\Delta G_{\text{ele, sol}}^{\text{d}}$	35.41 ± 2.04	40.59 ± 2.24
$\Delta G_{\text{bind, prede}}^{\text{e}}$	-29.00 ± 2.53	-32.23 ± 1.98

^a ΔG_{ele} , electrostatic interactions calculated using the MM force field.

^b ΔG_{vdw} , van der Waals' contributions from MM.

^c $\Delta G_{\text{nonpol, sol}}$, the nonpolar contribution to solvation.

^d $\Delta G_{\text{ele, sol}}$, the polar contribution to solvation.

^e $\Delta G_{\text{bind, pred}} = \Delta G_{\text{ele}} + \Delta G_{\text{vdw}} + \Delta G_{\text{nonpol, sol}} + \Delta G_{\text{ele, sol}}$, the predicted binding free energies with the entropic contribution omitted.

Figure Captions

Fig. 1. Workflow of the virtual screening process, combining the pharmacophore model screening, molecular docking, MD simulations, and bioassay. Nine hits were identified as PDE2 inhibitors in further bioassay.

Fig. 2. The pharmacophore model used in the screening of PDE2A inhibitors (1) and the pharmacophore model mapped with the ligands in the training set (2). Don|Acc: hydrogen bond donor or acceptor; Acc2|Don2: projection of the acceptor or the donor; Don|Acc|Hyd: a unified feature of the Don|Acc or the hydrophobic centroid one; PiR|Aro: Pi ring center or aromatic center; Hyd|PiR: hydrophobic centroid or Pi ring center; PiN: normal ring center. The exclusion feature is not represented in the figure.

Fig. 3. Chemical structures and affinities of the nine PDE2A inhibitors along with their SPECS IDs.

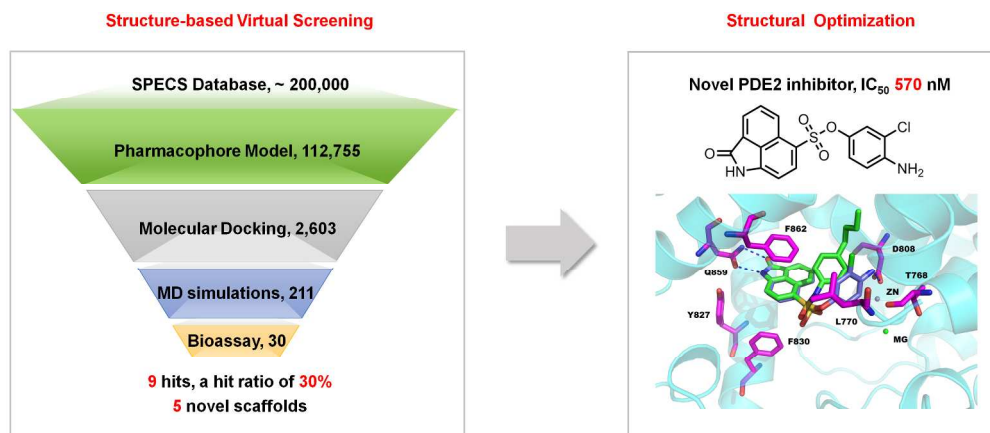
Fig. 4. The inhibitory profiles of hit compounds **AQ-390/10779040** and **AG-690/10776061** on PDE2A.

Fig. 5. Binding modes of four most representative inhibitors within the active site pocket of human PDE2A (PDB ID: 4HTX, color in cyan, key residue in magenta) after 8 ns MD simulations. The molecules (carbon in slate, oxygen in red, sulfur in yellow, nitrogen in blue and chlorine in green) are AQ-390/10779040 (1), AG-690/10776061 (2), AG-670/40741585 (3), and AG-690/12244899 (4), respectively. Hydrogen bonds are represented by dash lines.

Fig. 6. The binding mode of **LHB-8** (carbon in slate, oxygen in red, sulfur in yellow, nitrogen in blue and chlorine in green) within the active site pocket of human PDE2A (PDB ID: 4HTX, color in cyan, key residue in magenta) after superposition on the binding pose of **AQ-390/10779040** (carbon in green, oxygen in red, sulfur in yellow and nitrogen in blue). Hydrogen bonds are represented by dash lines.

Fig. 7. Decomposition of the key residue contributions to the binding free energies for the complexes of PDE2 with **AQ-390/10779040** and **LHB-8**.

Scheme 1. Reagents and conditions: a) Chlorosulfonic acid, rt, 6h; b) Pyridine, rt overnight.



Graphic content

743x320mm (96 x 96 DPI)

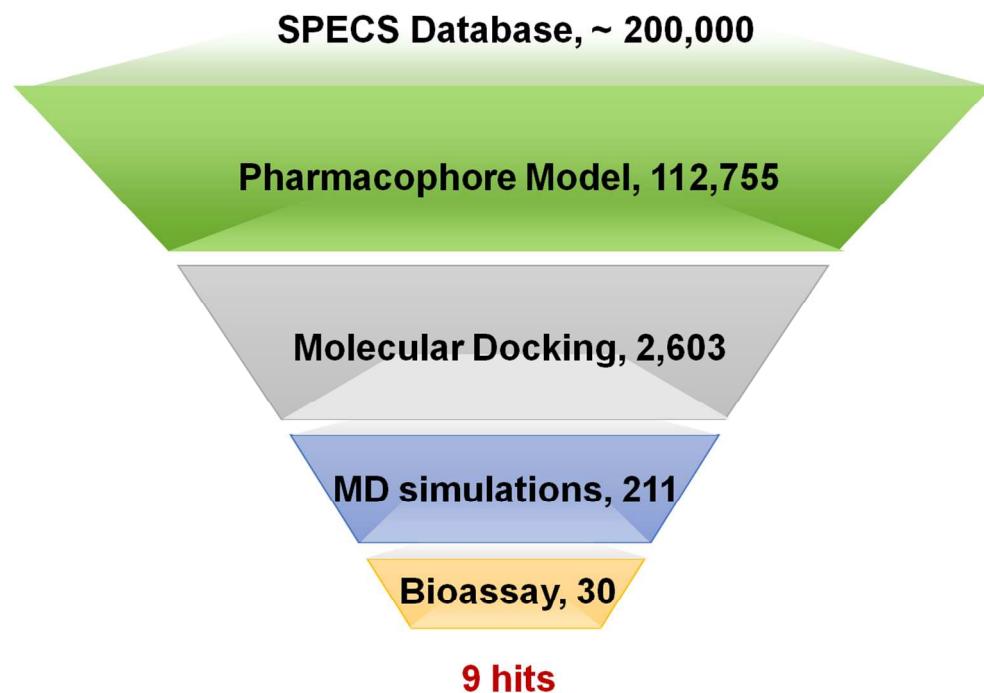


Fig. 1. Workflow of the virtual screening process, combining the pharmacophore model screening, molecular docking, MD simulations, and bioassay. Nine hits were identified as PDE2 inhibitors in further bioassay.

339x235mm (96 x 96 DPI)

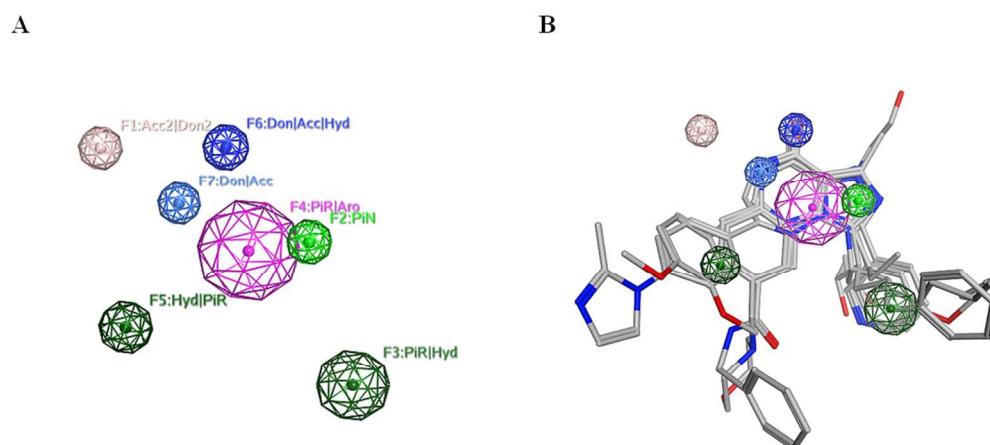


Fig. 2. The pharmacophore model used in the screening of PDE2A inhibitors (A) and the pharmacophore model mapped with the ligands in the training set (B). Don|Acc: hydrogen bond donor or acceptor; Acc2|Don2: projection of the acceptor or the donor; Don|Acc|Hyd: a unified feature of the Don|Acc or the hydrophobic centroid one; Pi|Aro: Pi ring center or aromatic center; Hyd|PiR: hydrophobic centroid or Pi ring center; PiN: normal ring center. The excluded volume features are not represented in the figure.

313x143mm (96 x 96 DPI)

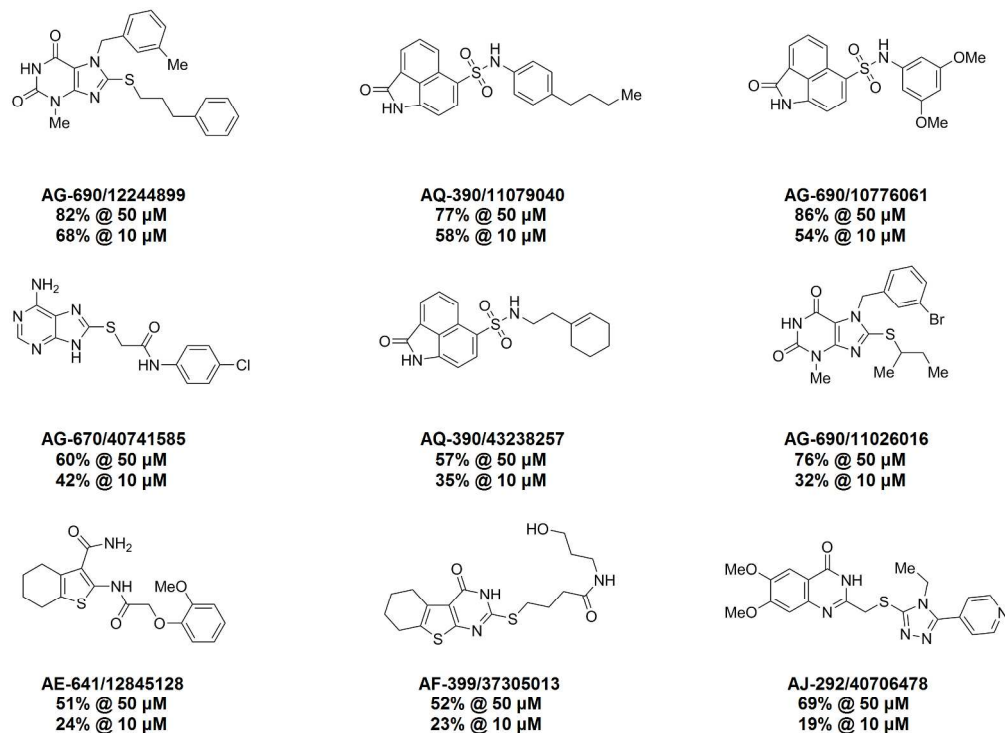


Fig. 3. Chemical structures and affinities of the nine PDE2A inhibitors along with their SPECS IDs.

727x573mm (96 x 96 DPI)

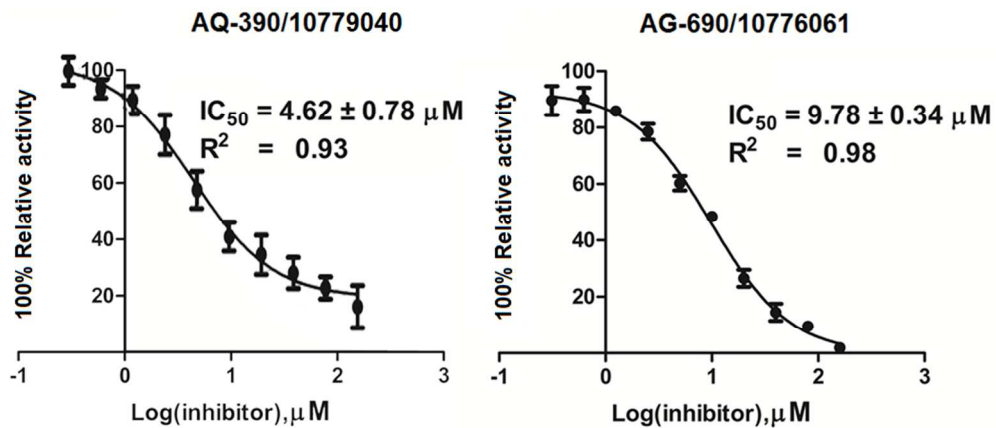


Fig. 4. The inhibitory curves of hit compounds AQ-390/10779040 and AG-690/10776061 towards PDE2A.

278x119mm (96 x 96 DPI)

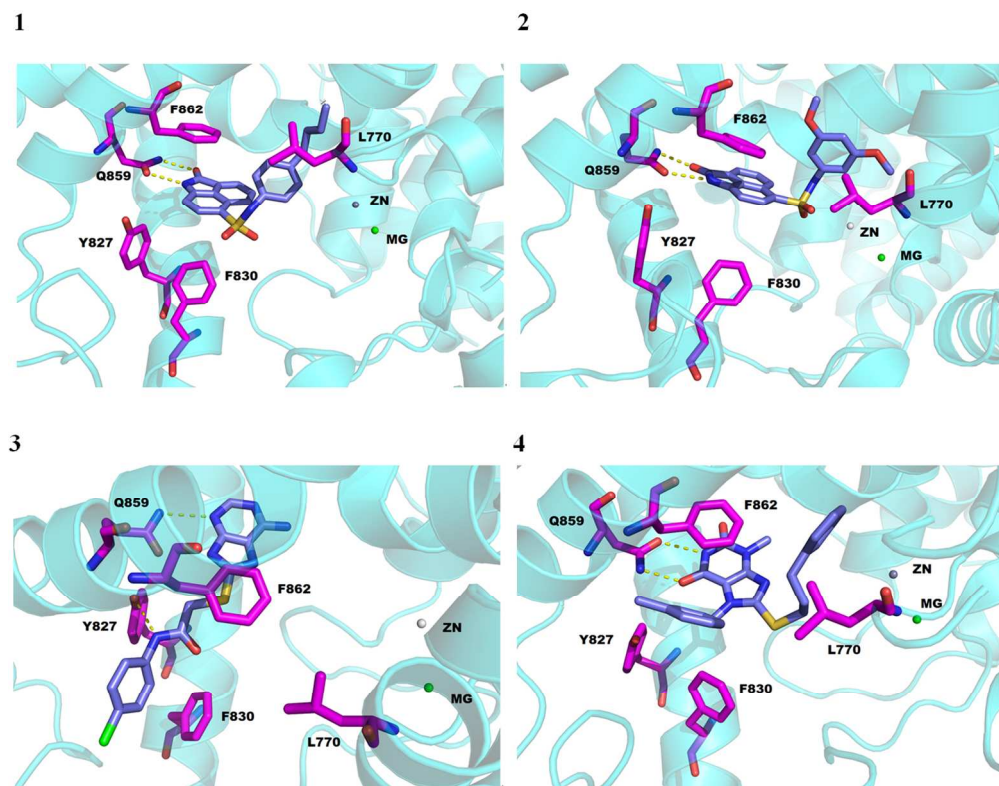


Fig. 5. Binding modes of four most representative inhibitors within the active site pocket of human PDE2A (PDB ID: 4HTX, color in cyan, key residue in magenta) after 8 ns MD simulations. The molecules (carbon in slate, oxygen in red, sulfur in yellow, nitrogen in blue, and chlorine in green) are AQ-390/10779040 (1), AG-690/10776061 (2), AG-670/40741585 (3), and AG-690/12244899 (4), respectively. Hydrogen bonds are represented by dash lines.

384x299mm (96 x 96 DPI)

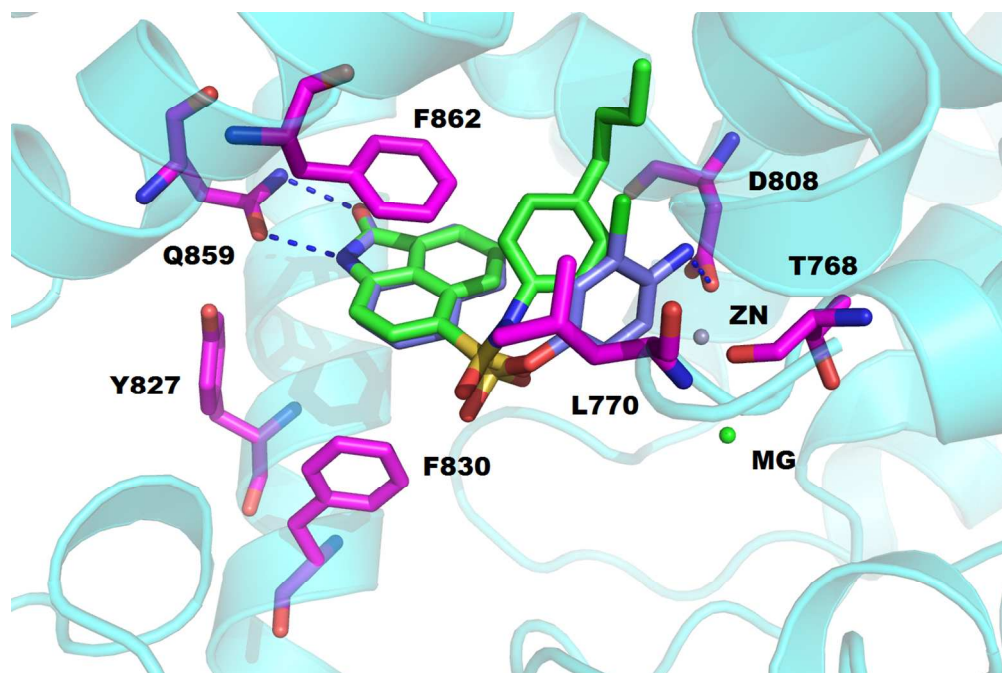


Fig. 6. The binding mode of LHB-8 (carbon inslate, oxygen in red, sulfur in yellow,nitrogenin blue and chlorine in green) within the active site pocket of human PDE2A (PDB ID: 4HTX, color in cyan, key residue in magenta) after superposition onthe binding pose of AQ-390/10779040 (carbon in green, oxygen in red, sulfur in yellow and nitrogen in blue). Hydrogen bonds are represented by dash lines.

386x256mm (96 x 96 DPI)

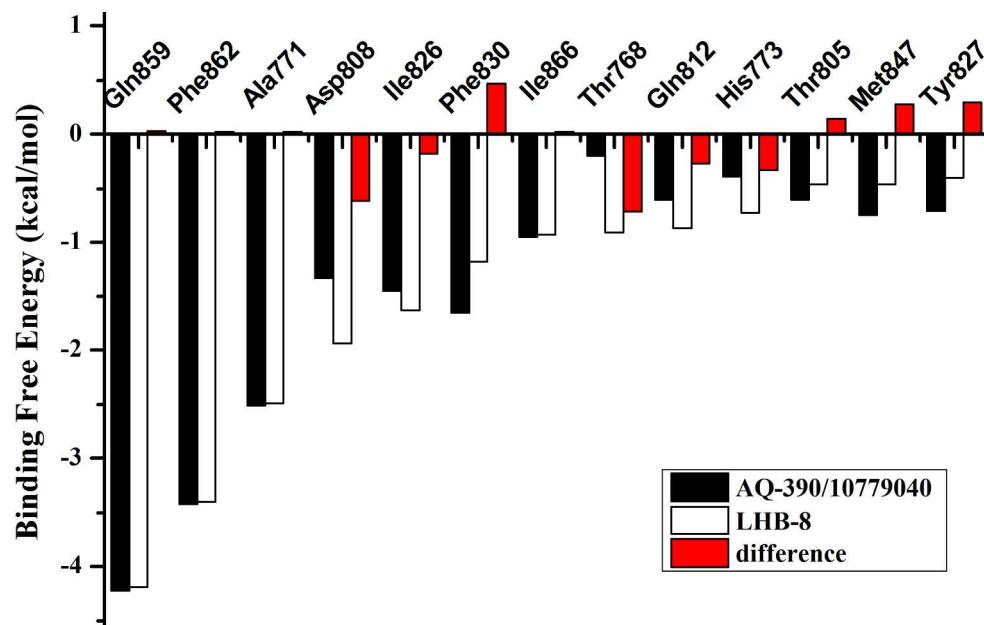
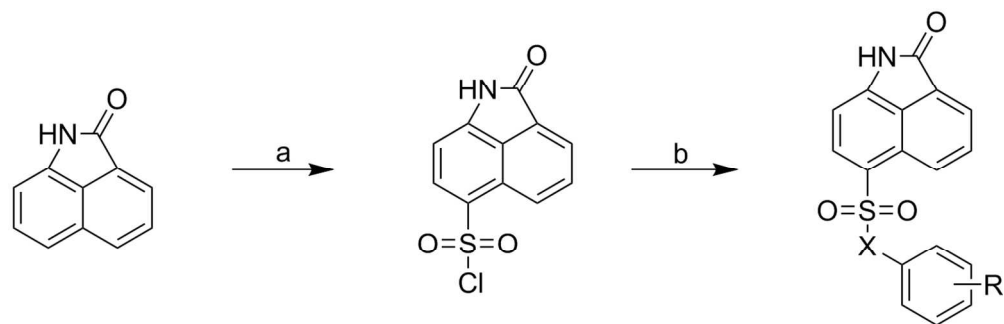


Fig. 7. Decomposition of the key residue contributions to the binding free energies for the complexes of PDE2 with AQ-390/10779040 and LHB-8.

223x138mm (300 x 300 DPI)



Scheme 1. Reagents and conditions: a) Chlorosulfonic acid, rt, 6h; b) Pyridine, rt overnight.

398x130mm (96 x 96 DPI)